Guest motion in tetrahydrofuran clathrate hydrate studied by deuteron nuclear magnetic resonance

A. Nowaczyk, B. Geil, S. Schildmann, and R. Böhmer
Fakultät für Physik, Technische Universität Dortmund, 44221 Dortmund, Germany
(Received 4 August 2009; revised manuscript received 18 September 2009; published 15 October 2009)

The guest dynamics in tetrahydrofuran (THF) clathrate hydrate ($THF \cdot 17H_2O$) was studied using several deuteron nuclear magnetic resonance (NMR) techniques. At low temperatures the magnetization recovery proceeds in two steps. The weight of the faster contribution decreases with decreasing temperatures. This behavior is the signature of a dynamical effect. The two contributions cannot be ascribed separately to the metadeuteron and to the paradeuteron of the THF molecule. The thermal evolution of the NMR spectra was described semiquantitatively using a distorted octahedral reorientational jump model. Pseudorotation has no significant impact on the spectral width. The motional correlation times, measured using two-time stimulated-echo and spin-relaxation techniques, cover a dynamic range of nine decades. Four-time stimulated-echo measurements reveal a statically heterogeneous rotational motion of the guest molecules in the 16-faced polyhedral cages of the structure II lattice.

DOI: 10.1103/PhysRevB.80.144303 PACS number(s): 82.75.−z, 76.60.−k, 33.15.Vb, 77.22.Gm

I. INTRODUCTION

Clathrates are a class of cage structures which, due to their "principle of construction," contain pores that are adapted to the size of the embedded guest molecules. In particular, for the clathrate hydrates with H_2O as the lattice-forming molecule, it is well known that larger cages form if larger guest molecules act as templates. The guests are usually translationally fixed leaving only rotational and intramolecular degrees of freedom to be observable. In that respect clathrates may be viewed analogous to orientationally disordered crystals. For this family of materials, with solid H_2, N_2, or CO as some of its simpler representatives,[1] only orientational motions persist somewhat below the melting point and, depending on the intermolecular interactions, they can freeze into a disordered configuration. The molecular slow down can be considered as a single-particle process in some of these substances[2] while in others they exhibit all the beauty and richness in behavior arising from varying degrees of intermolecular cooperativity.[3]

A somewhat different sterical confinement for small guest molecules can be achieved by zeolites.[4] From the perspective of the guests, this class of compounds contains hard-walled cages. These are limited by polygonal faces acting as windows with a spatial extension that can be tailored chemically. Furthermore, the mostly inorganic frame work of zeolites typically involves ions that exert specific interactions on the guests thereby giving rise to the catalytic properties for which these systems are frequently technologically exploited. Depending on the ratio of the guest-to-window size the cage-to-cage transport may be facilitated or strongly hindered. Benzene in certain zeolites[5] constitutes an example of confinement of basically single molecules so that the guest-to-wall interaction dominates. This "hard" confinement provides an environment for the enclosed molecular species which is relatively well geometrically defined. This situation is to be distinguished from soft confinements in which the host, often a glass forming material, exhibits an amorphous structure.

In clathrates, the impact of various interactions on the dynamics of the guests within the structure II (sII) hexakaidecahedral cages[6] is still not fully clarified. This is also true for the tetrahydrofuran (THF) clathrate hydrate, $THF \cdot 17H_2O$, which is in the focus of the present work. Some authors emphasized that the electrical fields set up by the proton disorder on the H_2O lattice play a vital role for the slowing down of the THF molecules[7] which itself carries an electrical dipole moment of $\mu_{THF}=1.63$ D.[8] Elastic interactions of the guests with the lattice are certainly important but simulations suggest that direct spatial THF-THF correlations are absent.[9] A recent nuclear magnetic resonance (NMR) study lent qualitative support to the idea that an interrelation exists between the host and the guest dynamics.[10] This disorder, shared by the THF guests and the clathrate water, may be causing the glasslike low-temperature thermal conductivity observed for $THF \cdot 17H_2O$.[11]

The relevance of disorder is also highlighted by the multitude of attempts to modify the degree of order on the water host structure, e.g., by doping it with ionic species such as KOH,[12,13] by hyperquenching,[14] or even by pressure-induced amorphization. When pressurizing $THF \cdot 17H_2O$ to 1.3 GPa at 77 K, the water structure has been reported to become similar to that of high-density amorphous ice.[15] Conversely, a tendency toward proton ordering can be achieved by doping the host lattice with tiny amounts of ionic defects.[12] Although it has been stated that "water molecules cannot be ordered in tetragonal symmetry while simultaneously obeying the ice rules"[16] the degree of order as estimated from the calorimetrically determined entropy[12] is somewhat below its theoretically possible value. Furthermore, strong local distortions of the cages were reported to appear in slightly KOH doped $THF \cdot 17H_2O$ at low temperatures ($T=5$ K).[16]

In the present work, we address the question regarding the interaction of the guests with the host lattice via a multidimensional deuteron NMR investigation thus complementing previous NMR studies which mostly exploited relaxometry, line-shape analysis, and double-resonance techniques.[10,14,17–27] Relatively broad, Gaussian-type NMR

spectra have been reported to occur at temperatures well above that at which the spin-lattice relaxation time T_1 is at its minimum.[25] A conclusion drawn from these experimental results is that "each THF molecule is surrounded by a slightly different water cage and the resultant distribution of local cage geometries confers differing degrees of anisotropic character on the reorientational motions of different THF molecules in the structure."[25] A quantitative justification of this time-honored idea[7,8] obviously has not been given.

Puckering motions of the THF molecules in the clathrate cages were claimed to be responsible for the observation of the Gaussian line shapes.[28] This intramolecular torsional mode, also called pseudorotation, is well known for THF from early infrared spectroscopy[29] as well as from electron diffraction.[30] It was intensively studied theoretically from first principles[31,32] and experimentally in various liquidlike and solidlike environments.[31,33–35] To detect the possible source of deuteron line shape blurring quadrupolar-echo double-resonance experiments were carried out and the role of heteronuclear dipolar interactions between the lattice protons and the deuterons of the guest molecules was emphasized.[14,25]

In the present work, we recorded solid-echo spectra (see Sec. III A) as well as spin relaxations (see Sec. III B) in order to monitor their evolution to lower temperature than accessible to previous studies and as a prerequisite to perform two- and four-time stimulated-echo experiments (see Sec. III C).

II. EXPERIMENTAL DETAILS

Some of the presently investigated clathrate hydrate samples with THF-d8 (=TDF, C_4D_8O) as guests were studied previously,[10] others were freshly grown. For these clathrates THF-d8 with a purity of 99.5% from Aldrich was dissolved in bidistilled H_2O so that the molar ratio TDF:H_2O was 1:17. This solution was supercooled to 4 °C and single crystals were grown by dipping a pipette containing a 77 K cold wire into this solution. The resulting single crystals were crushed under liquid nitrogen with a mortar and a pestle and hermetically sealed in glass tubes. No differences were found for the two sets of samples. The NMR experiments were performed at a Larmor frequency of 46.46 MHz using a home-built spectrometer. The $\pi/2$ pulses were typically 4.0 μs long. Spectra were obtained using the solid-echo sequence and corrected for finite pulse lengths.[36] Spin-spin relaxation times were also determined by applying a solid-echo pulse sequence. Spin-lattice relaxation times were measured subsequent to the application of a saturation comb. Two- and four-time stimulated-echo experiments were performed as described elsewhere.[37]

III. EXPERIMENTAL RESULTS

A. Deuteron NMR spectra

The main focus of the present work is to study the reorientational motion of the fully deuterated THF guests. More specifically our investigation relies on monitoring the orientation dependence of the quadrupolar frequency ω of the deuteron in the molecular C-D bonds which can be written as

$$\omega = \pm \tfrac{1}{2}\delta(3\cos^2\theta - 1). \tag{1}$$

Here θ denotes the angle which the C-D bond direction encloses with the external static magnetic field. The two signs account for the $0 \leftrightarrow 1$ and the $-1 \leftrightarrow 0$ transitions which occur for $I=1$ systems. The anisotropy parameter $\delta = 3e^2qQ/(4\hbar)$ is a measure for the strength of the quadrupolar coupling.

One can map out the orientational distribution of the NMR frequencies and thus of the C-D bonds by recording one-dimensional NMR spectra. For isotropic distributions typically Pake-type line shapes are obtained in the slow-motion limit, i.e., when the molecular correlation times τ are much longer than the inverse coupling, $\tau \gg \delta^{-1}$. In the presence of molecular dynamics motional narrowing sets in and yields characteristic line-shape changes. Eventually, for fast isotropic motion with $\tau \ll \delta^{-1}$, sharp Lorentzian line shapes are obtained.

We recorded ^{2}H solid-echo spectra of TDF·17H_2O thus extending previous measurements[17,21,25,26,40] to lower temperatures. Spectra are depicted in Fig. 1 for several temperatures. At $T=15$ K a spectrum with a rigid-lattice width of $\delta = 2\pi \times 123.3$ kHz is seen, then the effects of motional narrowing set in and for $T \geq 40$ K a relatively broad Gaussian line-shape emerges. In a first step, we fitted these line shapes using the expression

$$I_{\mathrm{Gauss}}(\omega) = \frac{1}{\sigma\sqrt{2\pi}}\exp\left(-\frac{\omega^2}{2\sigma^2}\right). \tag{2}$$

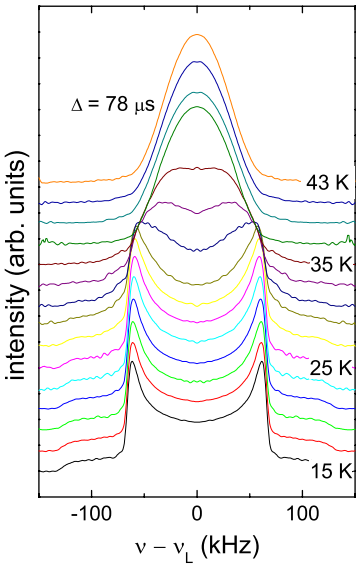

FIG. 1. (Color online) Solid-echo spectra of TDF·17H_2O recorded for an interpulse delay $\Delta = 78$ μs. When increasing the temperature from 15 to 43 K in steps of 2 K the Pake pattern successively transforms into a Gaussian line shape. Even close to the temperature at which the T_1 minimum appears its full width at half maximum is on the order of 26 kHz indicating a significant inhomogeneous broadening.

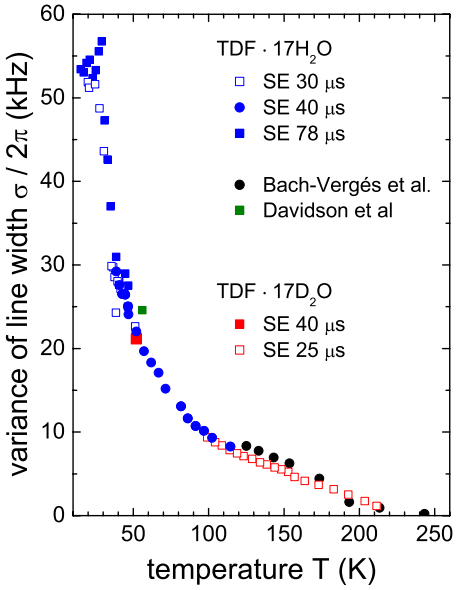

FIG. 2. (Color online) Standard deviation $\sigma(T)$ of the ^{2}H solid-echo spectra from this work in comparison with data from Bach-Vergés *et al.* (Ref. 25) and Davidson *et al.* (Ref. 21). For $T>35$ K σ is independent of the solid-echo delay Δ. The widths of the spectra from TDF·17H_2O agree with those from the guest molecules of TDF·17D_2O. This indicates that the ^{1}H-^{2}H dipolar interactions are not a significant source of line broadening in the lattice-protonated samples.

The resulting standard deviation σ is plotted in Fig. 2 as a function of temperature also including data from literature.[17,25] To be able to incorporate the information from the spectra measured at lower temperatures we determined their second moments numerically. For the Pake spectra showing up at the lowest temperatures we used $\sigma=\delta/\sqrt{5}\approx 0.447\delta$ applicable for an asymmetry parameter $\eta=0$.[38,39]

Coming from high temperatures the width σ first increases significantly between 125 and 200 K reaching values of about 8 kHz. This increase takes place in a range in which the molecular motion on the H_2O lattice freezes. Below about 100 K the width of the spectra increases rapidly which obviously is associated with the slow down of the TDF molecules.

It has been argued that a significant fraction of the deuteron linewidth is due to the heteronuclear magnetic dipole interactions of the TDF guests with the water protons. Therefore, we measured a fully deuterated TDF·17D_2O sample at temperatures for which the spin-lattice relaxation times of the two types of deuterons are sufficiently well separated so that the spectral contributions of the D_2O molecules could easily be suppressed. The linewidth of the TDF guest deuterons is included in Fig. 2 and seen to be identical to that obtained for the samples with a protonated lattice. This rules out magnetic dipole interactions as the dominant source of deuteron line-shape broadening. Otherwise the linewidth of the lattice-protonated sample should reflect that the dipolar interaction between host and guest deuterons are sixfold stronger ($\gamma_H/\gamma_D\approx 6$) than in the lattice deuterated specimen.

B. Spin-lattice relaxation

The dynamics of the THF guests has previously been studied by deuteron[25,27] and proton[17,19] spin-lattice relaxation times: A T_1 minimum shows up for TDF·17H_2O near 40–50 K, depending on the Larmor frequency. Below these temperatures the longitudinal magnetization recovery develops a strong nonexponentiality. In the low-temperature range the T_1 data have been fitted by various authors either using a stretched-exponential magnetization function[27] or using a sum of several distinct T_1 contributions,[25] e.g., to be related with the existence of chemically inequivalent deuterons, i.e., the four orthodeuterons (close to the oxygen atom) and the four metadeuterons.[40] In this context some authors emphasized the role of heterogeneous T_1 distributions[7] while others raised the possibility of a homogeneous scenario.[27] In the light of these discussions a careful reinvestigation of spin relaxation in TDF·17H_2O seems warranted.

Longitudinal magnetization recoveries were measured using the saturation recovery technique. Below the temperature of the T_1 minimum the data were fitted using a sum of two stretched exponentials

$$M(t)=M_0\{(1-R_f)\exp[-(t/T_{1s})^{1-\nu_s}]+R_f\exp[-(t/T_{1f})^{1-\nu_f}]\}. \tag{3}$$

We imposed the constraint $T_{1f}<T_{1s}$ since below the T_1 minimum the slower process (longer correlation times τ) is associated with the longer T_1 component. The stretching exponents ν_s and ν_f characterize the deviations from exponential spin-lattice relaxation and the factor R_f measures the fraction of the rapidly relaxing component. In Fig. 3 we summarize parameters obtained from least-squares fits for which we fixed the stretching exponents ν_s and ν_f to values of 0.45 and 0, respectively. In frame (a) it is seen that below 50 K T_{1f} and T_{1s} monotonously decrease with increasing temperature. A more pronounced variation appears in the range from about 25 to 35 K. Furthermore, the fraction R_f of the fast T_1 component decreases with a more rapid "drop," again in the same temperature range. A comparison with the standard deviation σ, as shown in Fig. 3(d), reveals that via the BPP expression

$$1/T_1=\tfrac{2}{15}\delta_{eff}^2[J(\omega_L)+4J(2\omega_L)] \tag{4}$$

this peculiar behavior is related with an ~50% increase in the effective quadrupolar coupling constant, δ_{eff}. In Eq. (4) $J(\omega_L)$ denotes the spectral density, i.e., the fluctuation probability for molecular motions occurring on the scale of the Larmor frequency. Another indication that the peculiar feature in the spin-lattice relaxation is due to a line-shape transition is obvious from Fig. 3(a). Here the spin-spin relaxation is seen to exhibit a minimum in the 25 to 35 K range signaling that the molecular motion takes place on the μs scale.

Like in previous work[40] the magnetization recovery of TDF·17H_2O was additionally fitted using a single stretched-exponential function yielding the mean relaxation time $\langle T_1\rangle$ [Fig. 3(a)] and a stretching exponent ν [Fig. 3(c)]. The exponent ν starts to become nonzero at ~95 K (at which $T_1\approx 0.3$ s), hence the underlying distribution of correlation times $g(\tau)$ becomes visible on this scale. Then ν passes

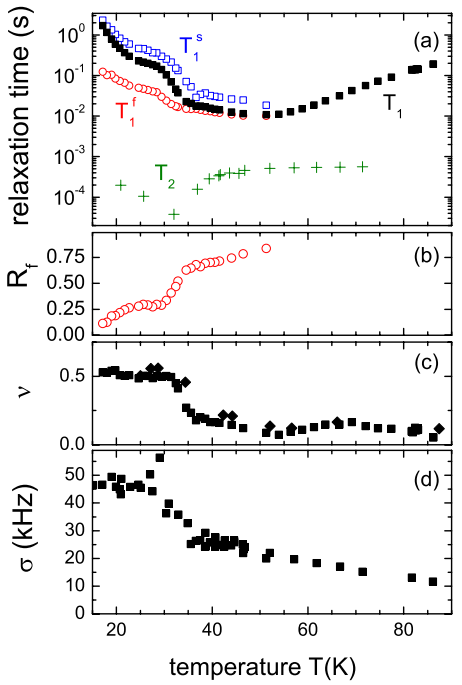

FIG. 3. (Color online) (a) Temperature dependence of the spin-lattice relaxation times T_1 and the transversal relaxation times T_2 as measured using the solid-echo sequence. The open symbols refer to the slow and fast contributions as analyzed using Eq. (3). Frame (b) shows the relative weight R_f of the fast component as defined in that equation. Fits using a single stretched-exponential function yielded the T_1 values shown as solid symbols in (a) and the stretching exponent ν presented in (c). The standard deviation σ of the linewidth is reproduced in (d) in an enlarged fashion in order to highlight that the "stepwise" change in the spectral width correlates with that in T_1 and in R_f as well as with the temperature range of the T_2 minimum.

through a maximum near 70 K. The decrease in ν at lower temperatures is related with the presence of a T_1 minimum and hence is artificial in the sense that it does not indicate a narrowing of the distribution of correlation times, $g(\tau)$.[41]

C. Stimulated echoes

To access longer motional time scales we utilize the stimulated-echo technique. Via appropriate application of three radio-frequency pulses one can determine the two-time correlation function

$$F_2(t_p,t_m,t_p) = \langle \cos[\omega_Q(0)t_p]\cos[\omega_Q(t_m)t_p]\rangle. \quad (5)$$

This function probes the molecular reorientation during the mixing time t_m. In the experiment the stimulated echo is additionally damped by spin-lattice relaxation, $M(t)$, which was measured independently and is corrected for in the data to be shown in the following. The resulting signal can be parameterized using

$$F_2(t_p,t_m) \propto A_1(t_p) + A_2(t_p)\exp\{-[t_m/\tau(t_p)]^\beta\}. \quad (6)$$

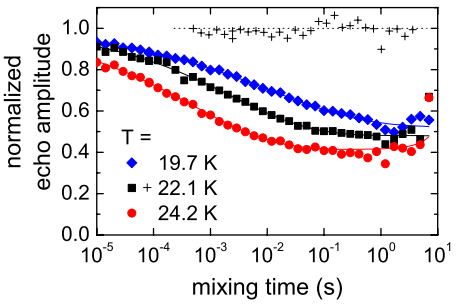

FIG. 4. (Color online) The circles represent normalized, T_1-corrected stimulated-echo intensities $F_2(t_m)$ as a function of the mixing time. The solid lines are fits using a stretched-exponential function decaying to a finite plateau value Z. The crosses represent an F_4 function with mixing times chosen as $t_{m1}=t_{m3}=1$ ms. The dashed line emphasizes that F_4 is 1 within experimental error. Two- and four-time stimulated-echo functions were recorded for evolution times of $t_p=20$ and 15 μs, respectively.

Here the coefficients $A_1(t_p)$ and $A_2(t_p)$ in general depend on the evolution time t_p and can be used to define the final-state amplitude ratio

$$Z(t_p) = A_1(t_p)/[A_1(t_p) + A_2(t_p)]. \quad (7)$$

For evolution times $t_p \to \infty$ this quantity is a measure for the number of magnetically distinguishable orientations each C-D bond can attain. Furthermore, $\tau(t_p)$ and β characterize time scale and stretching of the two-time correlation functions, respectively.

In Fig. 4 we show the temperature dependence of these functions for $t_p=15$ μs. From the decay of $F_2(t_m)$ the correlation time τ_2 can be read off and the long-time limit of $F_2(t_m \to \infty)$ immediately yields Z. One recognizes that the time scales τ_2 become longer when lowering the temperature and that Z is close one half. The stretching parameter β was 0.28 ± 0.02 and showed no systematic temperature dependence. This exponent corresponds to a width of correlation times of approximately three decades.

Evolution time-dependent results are presented in Fig. 5 for several temperatures. Above 20 K the relaxation times do not strongly depend on t_p indicating that relatively large jump angles dominate the reorientational behavior.[42] In frame Fig. 5(b) it is seen that Z exhibits values in the range 0.43 ± 0.1 with a modulation period which is characteristic for the presence of a unique quadrupolar coupling. Usually $Z^{-1}(t_p \to \infty)$ gives the number of magnetically inequivalent sites and therefore one may conclude that two to three distinguishable orientations can be reached by each C-D bond.[43]

The strong nonexponentiality of the molecular correlation function was further investigated using the four-time function

$$E_4(t_{m1},t_{m2},t_{m3}) = \langle \cos(\omega_1 t_p)\cos(\omega_2 t_p)\cos(\omega_3 t_p)\cos(\omega_4 t_p)\rangle. \quad (8)$$

In the presence of a rate exchange, i.e., when slow molecules become fast and vice versa during the mixing time t_{m2}, a

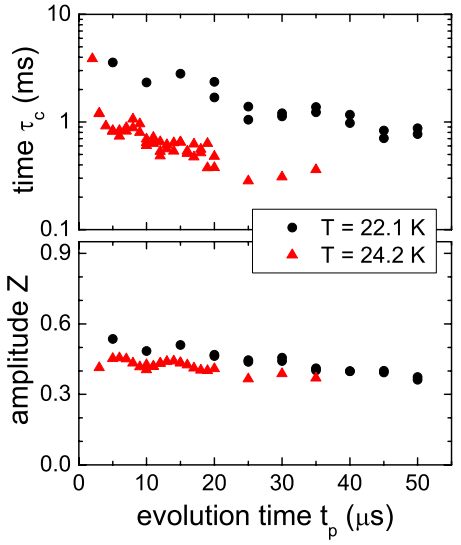

FIG. 5. (Color online) Evolution time dependence of the parameters $\tau(t_p)$ (frame a) and $Z(t_p)$ (frame b) resulting from stretched-exponential fits to the $F_2(t_m)$ functions. For the fits $\beta \approx 0.3$ was kept constant.

decay occurs in $F_4(t_{m2}) = E_4(t_{m1} = \text{const}, t_{m2}, t_{m3} = t_{m1})$. Measurements of $F_4(t_{m2})$ allow one to determine the time scale on which such a slow↔fast exchange takes place. This feature was previously exploited to characterize the dynamics of polymers,[44] supercooled liquids,[45] disordered molecular crystals,[46] ion conductors,[47] as well as the lattice dynamics in clathrates.[48] In Fig. 4 an $F_4(t_{m2})$ function, recorded at 22.1 K is shown and seen to be constant within the experimentally accessible range of mixing times. This means that dynamical exchange could not be detected. In other words, the stretching seen in F_2 is due to a statically heterogeneous distribution of correlation times.

IV. DISCUSSION

Of particular interest in the present study are the factors governing the motional geometry and dynamics of the THF guests in their hexakaidecahedral water cages. Before dealing with geometrical aspects of this motion let us first summarize the information about the guest correlation times τ_c from various experimental methods. Among them the stimulated-echo technique yields τ_c in a model-free way. In Fig. 6 we show the $1/e$ decay times of the F_2 functions. Another straightforward determination of $\tau_c = A/\omega_x$ is from the minima in the spin-lattice relaxation time [$A = 0.62$, $\omega_x = \omega_L = (3.43\ \text{ns})^{-1}$] and in the spin-spin relaxation time [$A = 1$, $\omega_x = \delta = (1.29\ \mu\text{s})^{-1}$]. Figure 6 documents that these τ_c values obey an Arrhenius law $\tau_c = \tau_0 \exp(E/T)$ with an activation energy of 496 K = 4.12 kJ/mol.[49] Using the high-temperature (HT) approximation of Eq. (4), $1/T_1 = \frac{2}{3}\tilde{\delta}_{eff}^2 \tau_c$, our T_1 data are compatible with this barrier also above the T_1 minimum if $\tilde{\delta}_{eff} = 2\pi \times 31$ kHz (see Fig. 6). This value corresponds to a standard deviation of $\tilde{\delta}_{eff}/\sqrt{5} \approx 2\pi \times 14$ kHz which is about the mean value of $\sigma/2\pi$ in the relevant temperature range, 50 K $< T <$ 100 K, see Fig. 2.

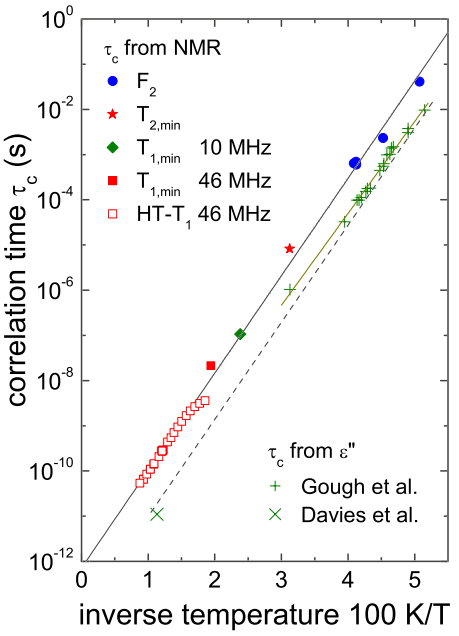

FIG. 6. (Color online) Arrhenius plot for the correlation times of the THF clathrate hydrate. The solid line represents an Arrhenius law with $E = 496$ K and $\tau_0 = 7.2 \times 10^{-13}$ s, the dashed line is parallel shifted by a factor of 10. The 10 MHz data are from Ref. 21, all other NMR results taken at 45 MHz are from this work. The high-temperature (HT) correlation times were obtained from $\tau_C = (\frac{2}{3}\tilde{\delta}_{eff}^2 T_1)^{-1}$ as described in the text. Dielectric loss (ε'') data by Davies *et al.* (Ref. 50) and Garg *et al.* (Ref. 19) are also included.

Figure 6 includes time constants determined for $T < 100$ K using dielectric spectroscopy.[13,50,51] Overall they indicate the same energy barrier against rotation of the THF molecule.[52] In spite of this similarity it is remarkable to find that the correlation times from dielectric spectroscopy are considerably shorter than those from NMR. Possible origins of this deviation were discussed previously.[19,21]

The specification of *mean* relaxation times is not sufficient to describe the guest dynamics fully. This is particularly obvious at low temperatures at which the spin-lattice relaxation is bimodal. It has been suggested that the two T_1 components arise from the deuterons at the orthoposition and the metaposition of the THF molecules, respectively.[40] In that case the relative magnitudes of R_f and R_s, see Eq. (3), should equal 0.5 independent of temperature but this is not observed, see Fig. 3(b). As mentioned below Eq. (4) the relatively strong variation in R_f between about 30–40 K is to be associated with an almost 50% change in the spectral width.

Among the various possibilities that come to mind when trying to rationalize such a change, let us first discuss the pseudorotation of the guest molecules. This kind of intramolecular motion was thoroughly studied in various phases of THF. From the freezing or thawing of only this type of motion we expect a maximum line shape change of about 20%, see Appendix A. On the other hand, it is clear that at $T \approx 15$ K the pseudorotation *is* frozen, otherwise the spectra at this temperature (see Fig. 1) would be narrower than the observed typical rigid-lattice linewidth. Is the activation of a puckering motion—on the NMR time scale—responsible for

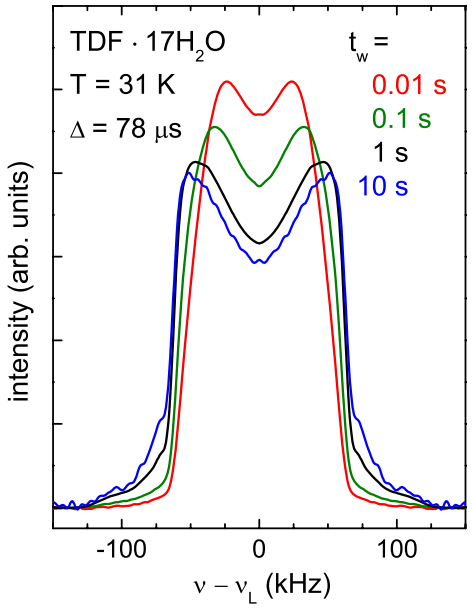

FIG. 7. (Color online) Partially and fully relaxed solid-echo spectra recorded a time t_w after saturating the nuclear magnetization.

the line shape observed upon heating through the 30 to 40 K range? Recalling that the line-shape variation is strongest in the range in which T_2 is close to its minimum, this would imply that the overall guest motion and the pseudorotation occur on about the same time scale which appears unlikely.[53]

What is the reason for the relatively abrupt change in linewidth? As evidenced by the stimulated-echo measurements, the THF motion is characterized by an enormously broad, statically heterogeneous distribution of correlation times. Under such conditions the occurrence of so-called two-phase spectra is expected.[54] Since the spectral change does not lead to a completely averaged line, we observe the "two-phase" character also in the weights of T_1.[55,56] As in related cases,[57] the slow T_1 contribution is expected to be associated with broader spectral components. We checked this conjecture by measuring spectra for variable waiting times t_w subsequent to saturation. The results are shown in Fig. 7. The second moment of the spectrum measured at 10 ms is indeed considerably smaller ($\sim$55%) than the fully relaxed spectrum.

It has been argued that the spectral profile and its progressive narrowing at higher temperatures is entirely due to the puckering motion of the THF molecule.[28] Furthermore, the Gaussian spectral shape obvious at $T>40$ K has been interpreted as the signature of incomplete motional narrowing without recourse to a distribution of quadrupolar coupling constants. However, since a Gaussian shape of significant width exists for temperatures far above the T_1 minimum, cf. Fig. 2, the interpretation of Ref. 28 is not tenable. Also one can exclude simple anisotropic motions of the THF molecules which in different cages lead to effective electric field gradient (EFG) tensors differing only in their asymmetry parameters η. This is because for a given quadrupolar coupling δ the edge singularities in deuteron spectra always appear at frequencies $\pm\delta$ independent of the special value of η. However, for $T>35$ K such edge features are obviously absent in the spectra observed in this work. Therefore, in agreement with previous approaches, a distribution $P(\delta)$ of effective anisotropy parameters δ is to be taken into account.[21,25] It was stated that the THF "molecules in different cages undergo reorientational motions which are not characterized by a common unique axis of rotation."[21] It is clear from the argument advanced in Ref. 21 that for each single molecule a fixed rotation axis was implied.

To describe this locally anisotropic motion quantitatively, it is worthwhile to point out that calorimetric data of slightly KOH-doped THF clathrate[12] as well neutron-scattering results suggest that each molecule can access six orientationally distinguishable sites, see Fig. 3 of Ref. 16. With this latter work as a starting point we discuss now what might be called the "distorted octahedral jump model." It refers to the quasi-C_2 axis of the THF molecule which is taken to point from its O atom to the midpoint of the opposite C-C bond. According to neutron data by Yamamuro *et al.*[16] this C_2 axis is preferably oriented along one of the six [100] directions of the cubic $Fd3m$ clathrate unit cell and the average plane of the THF molecule is parallel to one of the six (0 1 1) mirror planes of the hexakaidecahedral cage. The [100] axes intersect the midpoint of the O-O bonds on those of the 42 edges of the cage which are simultaneously vertices of two hexagonal and two pentagonal faces. The intersection points form a regular octahedron, i.e., a body with cubic point symmetry $\bar{4}3m$.[6] If the possible orientations of each C-D bond, or more precisely of each deuteron EFG tensor, conform to this octahedral symmetry then the average tensor has vanishing anisotropy and no quadrupolar splitting is observable for the deuteron resonance. However, each of the 42 O-O bonds is decorated with a proton which is shifted away from the midpoint of that bond thus disturbing the overall cubic symmetry. There is an enormous number of proton configurations which are compatible with the ice rules. The distributions of dipolar and quadrupolar *electrical* fields resulting for the sII structure have probably first been calculated by Davidson.[7]

In the present NMR context we are not concerned with the distribution of charges directly since the EFG tensors depend practically exclusively on the electron density within each C-D bond. However, the proton disorder in conjunction with point defects and lattice distortions will give rise to deformations of the rotational potential experienced by the THF molecule.[58] Attractive forces between its ether oxygen and the cage protons, akin to weak hydrogen bonds could also be relevant in that respect.[59] As a result deviations from the octahedral orientations of the C_2 axis will occur that are energetically less favorable than the ideal ones. Hence, with increasing temperature other molecular orientations and/or less preferred molecular plane alignments will become thermally populated and will impact on the overall symmetry that is relevant for a description of the guest motion.

In order to mimic the distortions of the 16-hedral cages we employed the model described in Appendix B: It is based on tilting away the octahedral axes from their ideal positions, on average by some angle $\alpha_{DOC}=\arctan(\sigma_{DOC}/r_0)$, which was quantified here by a standard deviation σ_{DOC} in terms of the typical "cage radius" r_0. The resulting distorted octahe-

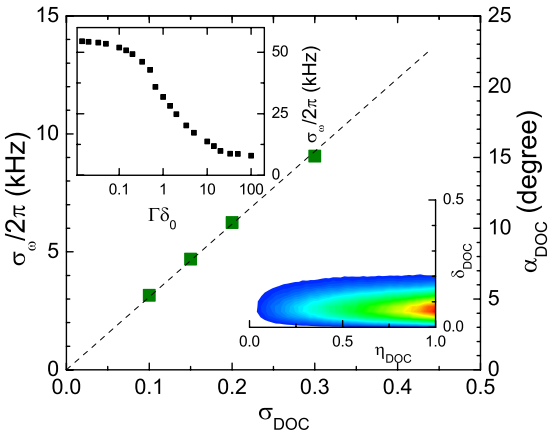

FIG. 8. (Color online) Parameters associated with the distorted octahedral jump model. The resulting spectral widths are proportional to the distortion of the octahedra as measured by σ_{DOC}. The lower inset shows a two-dimensional representation of the distributions of the anisotropy and asymmetry parameters underlying the spectral shape for $\sigma_{\mathrm{DOC}}=0.2$. The effects of an incomplete line narrowing as induced by a finite jump rate Γ are quantified in the upper inset for the same σ_{DOC}.

dral cages (DOCs) can thus be described by field gradient tensors with nonzero anisotropy and asymmetry parameters. The two-dimensional distribution (δ,η) of these quantities was obtained by numerical diagonalization of the tensors for a sufficiently large number of DOCs. The results are shown in the lower inset of Fig. 8. The distribution of η is seen to contain a large contribution near $\eta=1$. Hence it is no surprise that the spectra obtained on the basis of these distributions are relatively unstructured. In fact they can be described well by a Gaussian profile with a standard deviation σ_ω which in turn is proportional to σ_{DOC}, as shown in Fig. 8. Overall this figure reveals that the typical distortion angle is

$$\alpha \approx 1.67\sigma_\omega\,^\circ/\mathrm{kHz}. \tag{9}$$

The widths of the simulated spectra thus correspond to the fast-motion limit. By identifying the widths σ of the experimental spectra (see Fig. 2) with those of the simulated ones, σ_ω, via Fig. 8 [or equivalently via Eq. (9)] the associated, typical distortion angle α can be determined. For example, at 90 K, at which $\sigma/2\pi\approx 10$ kHz (cf. Fig. 2), the typical distortion angle is about 17°.

As also detailed in Appendix B, incomplete line-narrowing effects, which come into play at lower temperatures, were implemented via random-walk simulations involving jumps among the distorted octahedral sites. The resulting standard deviation σ_ω is shown as a function of the jump rate Γ in the upper inset of Fig. 8 for $\sigma_{\mathrm{DOC}}=0.2$. One recognizes that the linewidth starts to narrow significantly as soon as the rate becomes smaller than the asymmetry parameter δ_0, as it should. In the limit of large Γ the linewidth above determined by numerical diagonalization is asymptotically approached. Since also the correlation times (and hence rates Γ) are distributed we have not attempted to disentangle the combined effects of them from those of the degree of incomplete narrowing and cage distortion.

V. SUMMARY

The guest dynamics in TDF·$17H_2O$ was studied using various deuteron NMR methods. For temperatures below about 50 K the spin-lattice relaxation is bimodal with temperature-dependent weights. This finding was discussed in terms of a two-phase picture which is also corroborated by the evolution of the NMR linewidth.

A distorted octahedral jump model was developed and applied to describe the broad Gaussian line-shapes emerging for $T>40$ K. This model is based on a quasistatic distortion of the octahedral cages and enables one to relate the observed linewidth with a typical distortion angle. The latter decreases with increasing temperature.

At $T<25$ K the reorientational motion of the guest molecules was studied directly using the stimulated-echo technique. On the basis of these experiments we are led to conclude that each deuteron has access to $2,\ldots,3$ magnetically distinguishable orientations. Together with the T_1 measurements the guest dynamics was monitored by NMR techniques over a range of nine orders of magnitude. The two-time stimulated-echo functions exhibit a considerable stretching indicative for a broad distribution of correlation times which is more than three decades wide. Measurements of four-time correlation functions reveal that this distribution is statically heterogeneous in nature.

ACKNOWLEDGMENT

Funding by the Deutsche Forschungsgemeinschaft under Grant No. Bo1301/7 is gratefully acknowledged.

APPENDIX A

The internal motion of the nonplanar, ringlike THF molecule, the so-called pseudorotation, is usually described via the distance z of the oxygen atom (indexed by $k=0$) and the carbon atoms $(k=1-4)$ perpendicular to the average ring plane. Following the treatment of Kilpatrick *et al.*[60] and Geise *et al.*[30] the puckering amplitude is called q so that the coordinates of the five ring atoms can be described by $z(k)=\sqrt{2/5}q\cos(4\pi k/5+\varphi)$. The angle φ is determined by constraints that arise from keeping the bond lengths and various bond angles fixed. We use the same values as previous authors[30,34] who also provide a graphical representation of the situation. To describe the conformational motion of the THF molecule a rotational potential $U(\varphi)=U_2\cos(2\varphi)+U_4\cos(4\varphi)$ was found to be useful so that each of the C-D bonds can be thought to move along the surface of a strongly deformed cone. Typical values seem to be $|U_2|=15$ kJ/mol and $|U_4|=3$ kJ/mol.[37] From various studies of THF in the gaseous, liquid, and solid phases q was found to lie between 0.3 and 0.45 Å, for a compilation see Ref. 34.

Considering that $U(\varphi)$ involves four minima it may suffice to parameterize the effective deuteron EFG tensor $\mathbf{Q}$ as a superposition of four terms, $\mathbf{Q}=\Sigma_{k=1\cdots4}p_k\mathbf{Q}_k$. Here the largest principal axis of $\mathbf{Q}_k$, defined by the anisotropy parameter δ_0, is taken to point along a C-D bond and $\mathbf{Q}_k$ is assumed to be axially symmetric, $\eta_0=0$. The population factors p_k can be calculated from the difference of adjacent potential-

energy minima via the principle of detailed balance. To estimate the *maximum* reduction in the anisotropy parameter it may suffice to assume that all p_k are identical. By diagonalizing the resulting **Q** for a puckering amplitude with $q=0.38$ Å we obtain the following effective parameters for the orthodeuteron and the metadeuteron: $\delta_{ortho}=0.83\delta_0$, $\eta_{ortho}=0.2$ and $\delta_{meta}=0.86\delta_0$, $\eta_{meta}=0.17$. We checked these values by numerical simulations along the lines described in Appendix B. Furthermore, for $q=0.38$ Å the opening angle of the cones, alluded to above, is between about 10 and 40°. The larger opening angle corresponds to effective parameters, for which a two-site jump gives[36] $\delta_{eff}\approx 0.82\delta_0$ and $\eta_{eff}\approx 0.21$ in rough agreement with the above values.

APPENDIX B

We simulated the distorted octahedral jump model described in Sec. IV as follows. Ideally and after a suitable transformation of the molecular frame, a C-D bond would be defined to be oriented along a vector $\vec{p}_0$ pointing from the midpoint M of the octahedron to one of its vertices P_0. As noted in the text the relative orientations of these vertices are given by those of the midpoints of the O-O bonds on those edges of the cage which are simultaneously vertices of two hexagonal and two pentagonal faces.

In the following r_0 (=4.4 Å) denotes the distance between the two points M and P_0. In order to mimic the distorted situation efficiently, a point P within a Gaussian "cloud" centered around P_0 was then determined. More precisely, (i) a point P_1 on the unit sphere around P_0 was selected at random to define the orientation of a vector and (ii) its length p was then chosen to satisfy the Gaussian distribution

$$G(p)=\frac{1}{\sigma_{DOC}\sqrt{2\pi}}\exp\left(-\frac{p^2}{2\sigma_{DOC}^2}\right), \tag{B1}$$

with σ_{DOC} designating the standard deviation of the distribution. Then, the vector pointing from M to P was taken as the direction of the principal axis of a C-D bond. These axes were then allowed to jump among six independently distorted octahedral directions with a rate Γ in order to generate a trajectory of NMR frequencies. NMR spectra were calculated from the trajectories of typically 10^6 randomly oriented and statically distorted octahedra up to rates $\Gamma\sim 10^{-8}$ s^{-1}.

For larger Γ, corresponding to higher temperatures, these dynamical simulations become very time consuming. It is more efficient to calculate the effective anisotropy and asymmetry parameters by numerically diagonalizing the tensors obtained for a large number of DOCs. By applying this procedure again to about 10^6 cages the distributions of these EFG parameters and thus δ_{DOC} and η_{DOC} could be mapped out as a function of σ_{DOC}. An example for the two-dimensional distribution $P(\delta_{DOC},\eta_{DOC})$ is shown as inset in Fig. 8. Then we calculated the spectra based on these parameters as a function of σ_{DOC}. It turned out that the computed line shapes exhibited an almost perfect Gaussian profile that could be parameterized with a standard deviation σ_ω. In Fig. 8 it is seen that $\sigma_\omega=c_\omega\ \sigma_{DOC}$, i.e., the two standard deviations are linearly related with an empirical constant $c_\omega=0.68$ kHz/Å.

We found that the distribution of angles $\alpha=\sphericalangle(\vec{p},\vec{p}_0)$ which resulted from the application of Eq. (B1), can be approximated by a sigmoidally shaped distribution. A typical angle characterizing the distortion of the octahedral symmetry is $\alpha_{DOC}\sim\arcsin(\sigma_{DOC}/r_0)\sim\sigma_{DOC}/r_0$ which in turn is linearly related to σ_ω. Figure 8 reveals this proportionality between α_{DOC} and σ_ω directly.

[1] N. G. Parsonage and L. A. K. Staveley, *Disorder in Crystals* (Clarendon, Oxford, 1978).
[2] S. B. Liu and M. S. Conradi, Phys. Rev. B **30**, 24 (1984).
[3] N. S. Sullivan, Bull. Magn. Reson. **18**, 265 (1997).
[4] J. Kärger and D. M. Ruthven, *Diffusion in Zeolites and Other Microporous Solids* (Wiley & Sons, New York, 1992).
[5] D. J. Schaefer, D. E. Favre, M. Wilhelm, S. J. Weigel, and B. F. Chmelka, J. Am. Chem. Soc. **119**, 9252 (1997).
[6] T. C. W. Mak and R. K. McMullan, J. Chem. Phys. **42**, 2732 (1965).
[7] D. W. Davidson, Can. J. Chem. **49**, 1224 (1971).
[8] D. D. Klug and E. Whalley, Can. J. Chem. **51**, 4062 (1973).
[9] S. Alavi, J. A. Ripmeester, and D. D. Klug, J. Chem. Phys. **124**, 014704 (2006) performed molecular-dynamics simulations of $THF\cdot 17H_2O$ at 12 MPa and 100 K.
[10] T. M. Kirschgen, M. D. Zeidler, B. Geil, and F. Fujara, Phys. Chem. Chem. Phys. **5**, 5247 (2003).
[11] J. S. Tse and M. A. White, J. Phys. Chem. **92**, 5006 (1988); A. I. Krivchikov, V. G. Manzhelii, O. A. Korolyuk, B. Ya. Gorodilov, and O. O. Romantsova, Phys. Chem. Chem. Phys. **7**, 728 (2005).
[12] O. Yamamuro, M. Oguni, T. Matsuo, and H. Suga, Solid State Commun. **62**, 289 (1987).
[13] O. Yamamuro, T. Matsuo, and H. Suga, J. Inclusion Phenom. **8**, 33 (1990).
[14] C. A. Tulk, Y. Ba, D. D. Klug, G. McLaurin, and J. A. Ripmeester, J. Chem. Phys. **110**, 6475 (1999).
[15] Y. Suzuki, Phys. Rev. B **70**, 172108 (2004).
[16] O. Yamamuro, T. Matsuo, H. Suga, W. I. F. David, M. Ibberson, and A. J. Leadbetter, Physica B **213–214**, 405 (1995).
[17] D. W. Davidson, *Water—A Comprehensive Treatise*, edited by F. Franks (Plenum, New York, London, 1973), Vol. 2, pp. 115–234.
[18] R. J. Hayward and K. J. Packer, Mol. Phys. **25**, 1443 (1973).
[19] S. K. Garg, D. W. Davidson, and J. A. Ripmeester, J. Magn. Reson. (1969-1992) **15**, 295 (1974).
[20] S. K. Garg, S. R. Gough, and D. W. Davidson, J. Chem. Phys. **63**, 1646 (1975).
[21] D. W. Davidson, S. K. Garg, and J. A. Ripmeester, J. Magn. Reson. (1969-1992) **31**, 399 (1978).
[22] M. Junio, D. O. Leicht, and M. D. Zeidler, Faraday Symp. Chem. Soc. **17**, 25 (1982).
[23] C. Albayrak, M. D. Zeidler, R. Küchler, and O. Kanert, Ber. Bunsenges. Phys. Chem. **93**, 1119 (1989).

[24] D. M. Jacobs, M. D. Zeidler, and O. Kanert, J. Phys. Chem. A **101**, 5241 (1997).
[25] Y. Ba, C. I. Ratcliffe, and J. A. Ripmeester, Chem. Phys. Lett. **299**, 201 (1999).
[26] M. Bach-Vergés, S. J. Kitchin, K. D. M. Harris, M. Zugic, and C. A. Koh, J. Phys. Chem. B **105**, 2699 (2001).
[27] T. M. Kirschgen, M. D. Zeidler, B. Geil, and F. Fujara, Phys. Chem. Chem. Phys. **5**, 5243 (2003).
[28] E. Meirovitch and J. H. Freed, Chem. Phys. Lett. **64**, 311 (1979).
[29] W. J. Lafferty, D. W. Robinson, R. V. St. Louis, J. W. Russell, and H. L. Strauss, J. Chem. Phys. **42**, 2915 (1965).
[30] H. J. Geise, W. J. Adams, and L. S. Bartell, Tetrahedron **25**, 3045 (1969).
[31] B. Cadioli, E. Gallinella, C. Coulombeau, H. Jobic, and G. Berthier, J. Phys. Chem. **97**, 7844 (1993).
[32] V. M. Rayon and J. A. Sordo, J. Chem. Phys. **122**, 204303 (2005).
[33] A. L. Esteban, M. P. Galache, E. Diez, J. San Fabian, and F. J. Bermejo, Mol. Phys. **69**, 429 (1990).
[34] C. Schmidt, M. E. Rosen, D. F. Caplan, A. Pines, and M. F. Quinton, J. Phys. Chem. **99**, 10565 (1995).
[35] S. Lusceac (unpublished).
[36] K. Schmidt-Rohr and H. W. Spiess, *Multidimensional Solid State NMR and Polymers* (Academic, London, 1994), p. 66.
[37] G. Hinze, R. Böhmer, G. Diezemann, and H. Sillescu, J. Magn. Reson. **131**, 218 (1998).
[38] J. Davis, Biochim. Biophys. Acta **737**, 117 (1983).
[39] R. Böhmer, B. Geil, and S. Faske, Solid State Nucl. Magn. Reson. **34**, 32 (2008).
[40] T. M. Kirschgen, Ph.D. thesis, Shaker Verlag, 2001.
[41] R. Böhmer, F. Fujara, and G. Hinze, Solid State Commun. **86**, 183 (1993).
[42] For $T<20$ K a $(t_p)^{-2}$ dependence was found already for $t_p>10$ μs, probably signaling the onset of spin diffusion.
[43] If motional phase averaging occurs, this can give rise to additional contributions to Z, see S. Berndt, K. R. Jeffrey, R. Küchler, and R. Böhmer, Solid State Nucl. Magn. Reson. **27**, 122 (2005).
[44] K. Schmidt-Rohr and H. W. Spiess, Phys. Rev. Lett. **66**, 3020 (1991).
[45] R. Böhmer, G. Diezemann, G. Hinze, and E. Rössler, Prog. Nucl. Magn. Reson. Spectrosc. **39**, 191 (2001).
[46] M. Winterlich, G. Diezemann, H. Zimmermann, and R. Böhmer, Phys. Rev. Lett. **91**, 235504 (2003).
[47] M. Vogel, C. Brinkmann, H. Eckert, and A. Heuer, Phys. Rev. B **69**, 094302 (2004).
[48] S. Schildmann, A. Nowaczyk, B. Geil, C. Gainaru, and R. Böhmer, J. Chem. Phys. **130**, 104505 (2009).
[49] The present value of 496 K=4.12 kJ/mol can be compared with some previously reported ones. For 50 K$<T<$140 K a ^{1}H study (Ref. 19) yielded a value of 3.85 kJ/mol and for 143 K$<T<$213 K a ^{2}H study (Ref. 26) gave 2.2 kJ/mol.
[50] M. Davies and K. Williams, Trans. Faraday Soc. **64**, 529 (1968).
[51] S. R. Gough, R. E. Hawkins, B. Morris, and D. W. Davidson, J. Phys. Chem. **77**, 2969 (1973).
[52] M. A. White and M. T. Machant, J. Phys. Chem. **89**, 1380 (1985) determined a value $E\approx 420$ K by separating the rotational C_p contribution from a vibrational background which was estimated from that of ice I_h.
[53] Since $|U_4|\sim 3$ kJ/mol, see Ref. 34 and/or Appendix A, it cannot be ruled out that the puckering motion freezes out simultaneously with the overall molecular motion.
[54] E. Rössler, M. Taupitz, K. Börner, M. Schulz, and H.-M. Vieth, J. Chem. Phys. **92**, 5847 (1990).
[55] H. A. Resing, J. Chem. Phys. **43**, 669 (1965).
[56] As a possible origin of this behavior we would like to mention that the degree of proton order could be different in different cages, akin to the situation in KOH-doped clathrate hydrates, see Refs. 12 and 16, and A. Nowaczyk *et al.* (unpublished).
[57] F. Qi, R. Böhmer, and H. Sillescu, Phys. Chem. Chem. Phys. **3**, 4022 (2001).
[58] K. A. Udachin, C. I. Ratcliffe, and J. A. Ripmeester, J. Phys. Chem. B **111**, 11366 (2007).
[59] S. Alavi, R. Susilo, and J. A. Ripmeester, J. Chem. Phys. **130**, 174501 (2009).
[60] J. E. Kilpatrick, K. S. Pitzer, and R. Spitzer, J. Am. Chem. Soc. **69**, 2483 (1947).